Journal of Functional Materials and Applied Engineering

Review Paper

Application of Black Titanium Dioxide and Its Composite Materials in Photocatalytic Degradation of Water Pollutants

Alejandra Morosky[1], Steven Winter[2], Moley Mabry[2,*]

[1] Université Paris-Saclay, INRAE, AgroParisTech, UMR SAD-APT, 75005 Paris, France
[2] Department of Infrastructure Engineering, The University of Melbourne, Parkville, Australia
*Corresponding author: amorosky@inrae.fr; S22winter@unimelb.edu.au; mm33@unimelb.edu.au

Abstract. Photocatalysis has demonstrated tremendous potential across numerous application fields owing to its high efficiency, environmental friendliness, and low cost. Conventional titanium dioxide (TiO_2), a widely utilized photocatalytic material, possesses a large bandgap, restricting its light absorption solely to the ultraviolet region. Furthermore, the rapid recombination of photogenerated electron-hole pairs in TiO_2 limits its photocatalytic efficiency. Introducing defects such as oxygen vacancies onto the TiO_2 surface yields black titanium dioxide (TiO_{2-x}), which enhances its response performance and quantum efficiency in the visible and near-infrared regions by narrowing the bandgap and increasing active sites, thereby improving photocatalytic activity. Consequently, the synthesis and modification of black titanium dioxide have emerged as prominent research hotspots. This review systematically examines the critical defect structures of TiO_{2-x} and their characterization methodologies, summarizes its synthesis routes, and discusses modification strategies. Furthermore, it provides a focused analysis of the applications of TiO_{2-x} and its composite materials in the photocatalytic degradation of aquatic pollutants, accompanied by an in-depth summary of degradation mechanisms. Finally, the challenges and opportunities confronting TiO_{2-x} and its composites in the future remediation of environmental water pollution are outlined.

Keywords: *black titanium dioxide; modified materials; photocatalysis; water pollutants; degradation mechanisms*

Received on 10 Apr 2022, Accepted on 15 June 2022, Published on 08 July 2022

1 Introduction

Photocatalytic technology is an eco-friendly technique that utilizes light energy to drive redox reactions on material surfaces [1], eliminating the need for additional chemical reagents or thermal energy, and demonstrating immense potential across various application fields [2]. Titanium dioxide has emerged as one of the most extensively investigated semiconductor photocatalysts, attributed to its economic viability, biological inertness, and straightforward synthetic accessibility [3-4]. Nevertheless, conventional white-phase TiO_2 exhibits a broad bandgap of 3.0–3.2 eV, confining its photon absorption exclusively to the ultraviolet spectral region and consequently limiting solar energy conversion efficiency. Moreover, intrinsic structural imperfections and surface metastable configurations within the material promote rapid recombination of photogenerated electron-hole pairs, thereby depleting available charge carrier populations and attenuating overall photocatalytic performance [5-7]. In 2011, Chen et al.[8] prepared black titanium dioxide (TiO_{2-x}, $0 < x < 2$) with oxygen vacancies via high-temperature and high-pressure hydrogen reduction of white TiO_2. Studies show that this material has a narrow bandgap of 1.54 eV, and the introduction of oxygen vacancies and Ti^{3+} significantly enhances its light absorption and photocatalytic performance. Hydrogenation forms a disordered core-shell layer with a thickness of approximately 1 nm on the surface, which "passivates" unsaturated bonds on the surface and improves material stability. The disordered structure, oxygen vacancies, and Ti^{3+} defects on the TiO_{2-x} surface endow it with a narrow bandgap, enabling photon absorption from the ultraviolet (UV) to near-infrared (NIR) regions. However, in practical applications, surface defects of TiO_2 may cause deactivation of active sites during photocatalysis, compromising its cycling performance. Although a narrower bandgap improves light absorption capacity, it may also reduce the separation efficiency of photogenerated electron-hole pairs [9]. To further optimize the quantum efficiency and cycling stability of TiO_{2-x}, strategies including metal loading, non-metal doping, and heterojunction

construction have been developed. In recent years, TiO_{2-x} and its composites have attracted extensive research attention for their outstanding performance in photocatalytic degradation of aquatic pollutants [10–11].

Based on relevant characterization techniques, this paper sorts out the key defect structures of TiO_{2-x}, summarizes its synthesis methods and modification strategies, focuses on analyzing the application of TiO_{2-x} and its composites in photocatalytic degradation of aquatic pollutants, and conducts an in-depth discussion of the degradation mechanisms. Finally, the challenges and opportunities facing TiO_{2-x} in the field of environmental water pollution control are proposed.

2 Defect Structures of TiO_{2-x} and Their Characterization Methods

2.1 Surface Disordered Structure

Hydrogenation and analogous reduction treatments modify the surface crystallographic architecture of TiO_2, generating a disordered superficial stratum superimposed upon a crystalline core, yielding a distinctive core-shell morphology. This amorphous shell is enriched with structural imperfections including oxygen vacancies, Ti^{3+} centers, Ti–H linkages, and hydroxyl functionalities, which collectively facilitate accelerated separation of photogenerated charge carriers, broaden the spectral absorption window, and amplify photon harvesting efficiency [12]. The existence of this surface-disordered TiO_{2-x} layer can be corroborated through high-resolution transmission electron microscopy, Raman vibrational spectroscopy, and X-ray diffraction characterization (Figure 1).

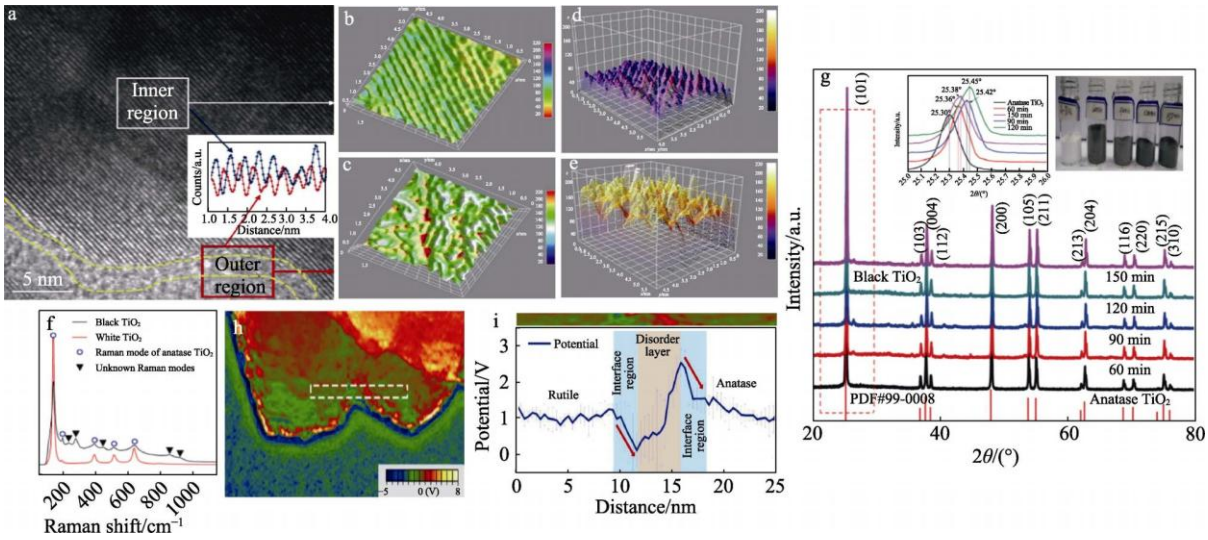

Figure 1 HRTEM image (a) and its 3D schematic diagram (b~e), Raman spectrum (f), electric potential diagram (h~i), XRD patterns (g) of TiO_{2-x} [13-18]

High-resolution transmission electron microscopy operates by transmitting an electron beam through the TiO_{2-x} specimen and forming magnified images via electromagnetic lens focusing. Through observation of lattice distortion and interplanar spacing modifications, the formation of the disordered shell within the core-shell architecture can be validated [13]. As depicted in Figure 1a, the yellow dashed demarcation surrounding the crystalline core denotes the surface disordered layer encasing the kernel, with an approximate thickness of 1 nm. Figures 1b and 1c display three-dimensional renderings of the internal crystalline core region highlighted by the white rectangle, revealing an atomically ordered planar surface; Figures 1d and 1e illustrate three-dimensional representations of the disordered shell region marked by the red rectangle, where long-range crystallographic ordering is disrupted, confirming the defective, amorphous nature of the outermost stratum [14]. Raman spectroscopy examines the inelastic light scattering behavior of TiO_{2-x}. As presented in Figure 1f, in comparison with pristine TiO_2 reference spectra, novel characteristic bands emerge at 238, 280, 447, 854, and 916 cm^{-1} for the reduced TiO_{2-x} phase [15], which are attributable to vibrational modes associated with the surface disordered configuration [16]. XRD determines the crystal structure by measuring the diffraction intensity of X-

rays irradiated on TiO_{2-x} at different angles. As shown in Figure 1g, the surface disordered layer destroys the crystal integrity, causing peak shifts. TiO_{2-x} shows good crystallinity, but the (101) characteristic peak shifts to the right with prolonged sintering time, indicating that the surface of reduced TiO_{2-x} samples undergoes disorder-induced lattice strain [17]. In addition, the potential diagrams of TiO_{2-x} (Figures 1h and 1i) show a sharp drop in potential at the interface between the crystalline and disordered regions, further confirming the formation of the surface disordered structure [18]. To clarify the structure-performance relationship between defect types in the surface disordered layer and the properties of TiO_{2-x}, a systematic analysis of the main defect types is necessary and meaningful.

2.2 Oxygen Vacancies and Ti^{3+}

Oxygen vacancies and Ti^{3+} in the surface disordered structure of TiO_{2-x} are the two most critical defect types affecting its performance. Oxygen vacancies are formed by the detachment of oxygen atoms from the lattice, mostly located on the material surface, which promotes the separation of photogenerated electron-hole pairs and thus improves photocatalytic reaction efficiency [19]. Density functional theory (DFT) simulations of TiO_{2-x} with different stoichiometries ($1.75 < x < 2.00$) show that the coordination number distribution of Ti atoms in TiO_{2-x} ranges from 5 to 7, while the average coordination number of oxygen increases with the deepening of the reduction degree, proving the existence of surface oxygen vacancies [20]. Ti^{3+} is mainly formed by the reduction of Ti^{4+} or oxidation of low-valent Ti atoms. Its incorporation engenders intermediate electronic states within the TiO_{2-x} band structure, compressing the bandgap and red-shifting the optical absorption threshold into the visible spectral domain, thereby substantially enhancing solar photon harvesting efficiency [21–23]. The existence of oxygen vacancies and Ti^{3+} centers can be characterized through ultraviolet-visible diffuse reflectance spectroscopy, X-ray photoelectron spectroscopy, Raman vibrational spectroscopy, and electron spin resonance techniques (Figure 2) [24–27].

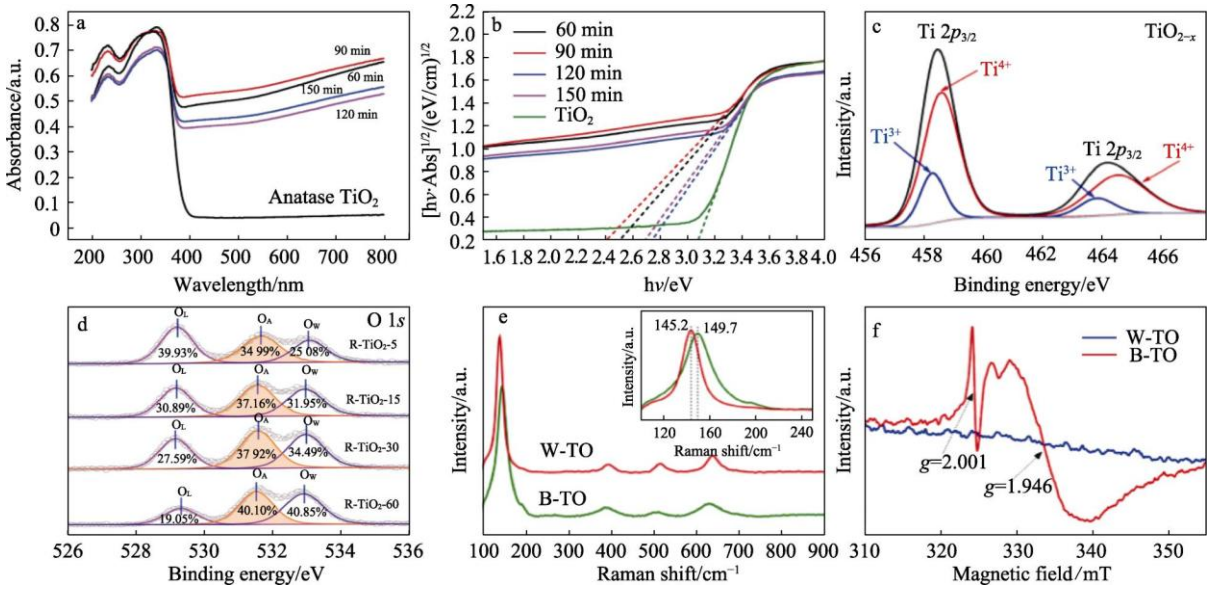

Figure 2 UV-Vis DRS (a,b), XPS (c,d), Raman (e), ESR (f) spectra of TiO_2 and TiO_{2-x} [24-27]

UV-Vis DRS irradiates TiO_{2-x} with ultraviolet light and measures the intensity and wavelength of scattered light. As illustrated in Figure 2a, Ti^{3+} presence induces discernible shifts in the optical absorption edge and associated spectral features. The bandgap energy of TiO_{2-x} can be derived through the Kubelka-Munk transformation, as presented in Figure 2b. The reduced material exhibits a bandgap of 2.4–2.8 eV, representing substantial narrowing relative to pristine TiO_2 (3.1 eV), thereby providing indirect evidence for oxygen vacancy formation [17]. XPS characterizes the energy level distribution and chemical state of TiO_{2-x} by analyzing the characteristic information of photoelectrons emitted when X-rays irradiate TiO_{2-x}. Figure 2c shows the distribution of Ti^{3+} among Ti atoms [25]; Figure 2d shows the proportion of oxygen vacancies [26], where OL, OA, and OWcorrespond to the absorption peaks of crystalline oxygen, oxygen vacancies, and adsorbed oxygen, respectively. Raman spectroscopy validates oxygen vacancy generation through characteristic peak perturbation

analysis: as depicted in Figure 2e, the principal Raman active mode of pristine white TiO_2 at 145.2 cm^{-1} exhibits a blue shift to 149.7 cm^{-1} upon reduction, with concurrent peak broadening confirming oxygen vacancy presence [27]. Oxygen vacancies and Ti^{3+} centers introduce supplementary electronic states harboring unpaired electrons, detectable through electron spin resonance spectroscopy. As shown in Figure 2f [27], the oxygen vacancy-associated signal appears at g = 2.001, while the resonance at g = 1.946 corresponds to surface Ti^{3+} species within the TiO_{2-x} matrix.

In summary, the core-shell structure of TiO_{2-x} and the oxygen vacancies and Ti^{3+} defects in its disordered shell positively affect photocatalytic performance [28]. However, it remains challenging to select appropriate synthesis methods and optimize synthesis conditions to precisely control the shell thickness and the contents of oxygen vacancies and Ti^{3+} in the disordered layer, so as to achieve optimal photocatalytic performance. Future research should combine the above characterization methods, select suitable synthesis routes and conditions to precisely regulate the structure, and finally realize ideal photocatalytic performance.

3 Synthesis Methods of TiO_{2-x}

The choice of synthesis method for TiO_{2-x} directly affects the distribution of oxygen vacancies and Ti^{3+}, as well as the bandgap width (Eg). Currently, TiO_{2-x} with regulated structures and bandgaps can be prepared via high-temperature calcination reduction, electrochemical synthesis, oxidation of low-valent Ti compounds, and other emerging methods, to obtain desirable photocatalytic performance.

3.1 High-Temperature Calcination Reduction Method

The high-temperature calcination reduction method reduces Ti^{4+} to Ti^{3+} and introduces oxygen vacancies under high-temperature conditions using reducing agents. This method significantly narrows the bandgap of TiO_{2-x} and improves its photocatalytic activity. Common reducing agents include H_2, $NaBH_4$, Al, Zn, Mg, CaH_2, and imidazole [8,29–39]. According to the type of reducing agent, it can be classified into H_2 reduction, plasma reduction, and other reduction processes. By adjusting temperature, pressure, atmosphere composition, and reducing agent type, TiO_{2-x} with different structures and bandgaps can be prepared. Table 1 summarizes the preparation conditions, bandgaps, and main structure types of TiO_{2-x} synthesized via high-temperature calcination reduction.

Table 1 TiO_{2-x} prepared by high temperature calcination reduction methods

Reduction method	Sample name	Preparation conditions	Eg / eV	Main structure type	Reference
H_2 reduction	TiO_{2-x} nanoparticles	Pure H_2, 2 MPa high pressure, 200 °C, 5 d	1.54	Oxygen vacancies, Ti^{3+}	[8]
	Mesoporous TiO_{2-x} hollow spheres	Pure H_2, atmospheric pressure, 600 °C, 3 h	2.59	Spherical, oxygen vacancies, Ti^{3+}	[29]
	TiO_{2-x} nanoparticles	H_2/N_2 mixed gas (8 vol% H_2), 700 °C	2.78	Oxygen vacancies, Ti^{3+}	[30]
	TiO_{2-x} nanorod arrays	H_2/Ar mixed gas (20 vol% H_2), 350 °C	—	Oxygen vacancies, Ti^{3+}	[31]
Plasma reduction	TiO_{2-x} nanoparticles	Hydrogen plasma, 500 °C, 8 h	2.05	Amorphous shell, oxygen vacancies, Ti^{3+}	[32]
	TiO_{2-x} film	H_2/Ar plasma, 300 °C	2.60	Oxygen vacancies, Ti^{3+}	[33]
Other reduction	TiO_{2-x} nanoparticles	N_2, $NaBH_4$, 350 °C	2.11	Oxygen vacancies, Ti^{3+}	[34]
	TiO_{2-x} nanoparticles	Vacuum, ethanol, 400 °C, 3 h	1.92	Oxygen vacancies	[35]
	TiO_{2-x} nanoparticles	N_2, NaN_3, 450 °C, 2 h	2.70	Oxygen vacancies, Ti^{3+}	[36]
	TiO_{2-x} nanoparticles	Vacuum, Al, 300–500 °C, 6 h	—	Spherical, oxygen vacancies, Ti^{3+}	[37]

Reduction method	Sample name	Preparation conditions	Eg / eV	Main structure type	Reference
	TiO_{2-x} nanoparticles	Vacuum, K, 140 °C, 1 h	0.45	Surface disordered shell, oxygen vacancies, Ti^{3+}	[38]
	TiO_{2-x} nanoparticles	Imidazole, 350 °C, 2 h	1.86	Oxygen vacancies, Ti^{3+}	[39]

3.1.1 H_2 Reduction

H_2 reduction treats white TiO_2 under specific pressure, temperature, and time conditions, using the reducing property of H_2 to replace O atoms to form oxygen vacancies, yielding TiO_{2-x}. Chen et al.[8] first treated white TiO_2 with pure H_2 at 2 MPa and 200 °C for 5 days to prepare TiO_{2-x} with a bandgap of 1.54 eV. Hydrogen incorporation generates intermediate electronic states bridging the conduction and valence bands, compressing the bandgap and extending the photon absorption window. Under identical experimental conditions, the photocatalytic performance of TiO_{2-x} approaches double that of unmodified TiO_2. Hu et al. [29] developed TiO_{2-x} hollow spheres through a template-free solvothermal approach combined with small amine molecule encapsulation and subsequent H_2 reduction (atmospheric pressure, H_2 atmosphere, 10 °C/min ramp to 600 °C, 3 h dwell), achieving a narrowed bandgap of 2.59 eV. The solar-driven hydrogen evolution rate [2410 μmol/(h·g)] substantially exceeded that of pristine TiO_2 [810 μmol/(h·g)] by approximately threefold. Zhang et al. [30] subjected TiO_2 to reductive treatment in an 8 vol% H_2/N_2 mixture at 700 °C, yielding TiO_{2-x} with a 2.78 eV bandgap; its hydrogen evolution performance under open-circuit conditions improved by nearly twofold relative to unmodified TiO_2 nanoparticles. Zhang et al. [31] fabricated TiO_2 nanorod arrays on fluorine-doped tin oxide-coated glass substrates through hydrothermal synthesis, followed by hydrogenation in a 20 SCCM H_2/80 SCCM Ar atmosphere (5 °C/min ramp to 350 °C). The resulting TiO_{2-x} nanorod photoelectrodes demonstrated visible-light photocatalytic organic degradation capability, with UV and visible region absorption enhancements of 4% and 50%, respectively. For the H_2 reduction process, regulating H_2 content, heating rate, temperature, and duration to control the hydrogenation degree of TiO_2 is instructive for determining the defect chemical properties. However, this method has high cost and risk, making it unsuitable for large-scale production.

3.1.2 Plasma Reduction

Hydrogen plasma treatment is usually carried out in vacuum or low-pressure environments, which is safer and more environmentally friendly than high-pressure H_2 reduction. Wang et al.[32] reduced TiO_2 in hydrogen plasma at 500 °C for 8 h, preparing TiO_{2-x} with a solar absorption rate of 83%. Studies show that the high absorption rate is induced by localized surface plasmon resonance (LSPR), which is closely related to the surface carrier concentration. This method introduces H doping and/or oxygen vacancies, converting surface Ti^{4+} ($3d^0$) to Ti^{3+} ($3d^1$), increasing the carrier (electron) concentration. Pylnev et al.[33] sputtered a conductive TiO_2 target in H_2/Ar plasma at 300 °C, obtaining TiO_{2-x} thin films with a bandgap reduced to 2.60 eV. During H_2 sputtering of the TiO_2 target, the structural evolution trend is: the XRD peak of anatase TiO_2 broadens, then partially transforms to rutile phase, then amorphizes, and finally converts to a crystalline intermediate oxide of Ti. Hydrogen plasma has high energy and can shorten the reaction time. Compared with direct use of H_2, it is more suitable for large-scale production of high-quality materials.

3.1.3 Other Reduction Methods

Other safer reducing agents can also be used to prepare TiO_{2-x}. Ariyanti et al.[34] mixed TiO_2 with $NaBH_4$ and heated the mixture to 300–450 °C in an Ar atmosphere in a furnace to obtain TiO_{2-x}. Results show that the material completely degrades rhodamine B (RhB) within 50 min, while traditional TiO_2 requires more than 90 min. Chen et al. [35] synthesized TiO_{2-x} exhibiting a bandgap of 1.92 eV through ethanol-mediated reduction of TiO_2 under vacuum at 400 °C for 3 h. Under equivalent experimental conditions, the photocatalytic methylene blue degradation efficiency of these TiO_{2-x} nanoparticles surpassed that of pristine TiO_2 nanoparticles by a factor of 1.8. Notably, this synthetic approach yielded TiO_{2-x} devoid of detectable Ti^{3+} species; oxygen vacancies alone functioned as mid-gap trapping centers to suppress photogenerated electron-hole pair recombination. Zheng et al. [36] prepared TiO_{2-x} via reaction of TiO_2 with sodium azide under nitrogen atmosphere at 450 °C for 2 h, achieving full-spectrum light harvesting capability. The resultant material demonstrated a water evaporation rate of 1.624 kg/(m^2·h), substantially exceeding the 0.515 kg/(m^2·h) observed for unmodified TiO_2. Wang et al.[37] used Al as the reducing agent and ordinary white TiO_2 as the raw material to prepare TiO_{2-x} in a dual-zone tube

furnace at 300–500 °C (the synthesis schematic is shown in Figure 3). The preparation principle is that O in pre-annealed TiO_2 is absorbed by molten Al, generating oxygen vacancies (Ov) on TiO_2. Al-reduced TiO_{2-x} absorbs about 60% more solar energy than pristine TiO_2. Lin et al.[38] used elemental K as the reducing agent to react with TiO_2 under vacuum, maintaining at 140 °C for 1 h, to prepare TiO_{2-x} with a bandgap of 0.45 eV. Under visible light irradiation, its photocatalytic degradation performance for MB is more than 300 times that of white TiO_2. Azab et al.[39] mixed TiO_2 and imidazole at a mass ratio of 1:2, added 3 mL of 37 wt% HCl solution, heated to 350 °C in a muffle furnace at a rate of 5 °C/min and maintained for 2 h, then heated at 400 °C for 1 h, to obtain TiO_{2-x} with a bandgap of 1.86 eV. For chemical reduction, regulating the mixing ratio, reaction temperature, and reaction time is required to control photocatalytic performance. This method avoids the use of H_2, and is a mild and convenient means for producing TiO_{2-x} powders and films.

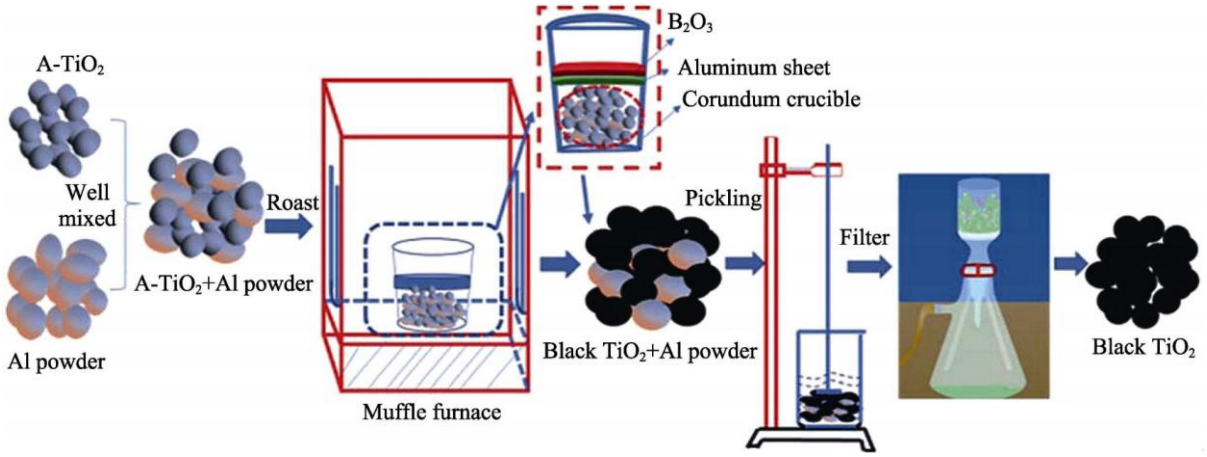

Figure 3 Schematic diagram of TiO_{2-x} synthezed by aluminum thermal reduction [37]

In general, traditional H_2 reduction requires high temperatures and long durations. Elevated temperature not only shortens the hydrogenation process and affects the defect types of the sample, but also adversely affects the sample skeleton. In addition, increased H_2 content leads to lattice expansion and reduced nanoparticle size, ultimately lowering the bandgap. Compared with traditional H_2 reduction, hydrogen plasma treatment does not require additional catalysts or solvents, and improves light absorption and photodegradation capacity due to the LSPR effect. However, the above methods all have high costs and are not suitable for large-scale production. The preparation of TiO_{2-x} using other reducing agents (such as $NaBH_4$, NaN_3) usually involves liquid-phase or solid-phase processes with more uniform grinding, and different reducing agents produce TiO_{2-x} with different structural defect types. Overall, using hydrides or other reducing agents to prepare TiO_{2-x} has the advantages of mild reaction conditions, low environmental pressure, high efficiency, low power consumption, and short time consumption. The preparation mechanisms of TiO_{2-x} can be summarized into two pathways: one is direct high-temperature reaction with the reducing property of H_2, ethanol, imidazole, etc., to reduce Ti atoms and gain electrons; the other is reduction of TiO_2 by strong reducing substances (such as H_2, metallic Na) decomposed at high temperature, such as $NaBH_4$ and NaN_3.

3.2 Electrochemical Synthesis Method

The electrochemical synthesis method usually uses titanium sheets as precursors, applies an external voltage in an electrolyte solution to trigger anodic oxidation on the electrode surface, generates TiO_2 nanotubes with abundant defects, and then heat-treats the product to prepare TiO_{2-x}. Qi et al. [40] employed titanium foil as the working electrode and platinum foil as the counter electrode, performing anodic oxidation for 1 h followed by thermal annealing at 450 °C for 2 h (5 °C/min heating rate) to fabricate a photoelectrode precursor. Subsequent 30 min electrochemical reduction was conducted to introduce Ti^{3+} centers and oxygen vacancies, yielding TiO_{2-x} with a narrowed bandgap of 2.7 eV and extended visible-light absorption. Li et al. [41] performed anodic oxidation of titanium sheets in an ethylene glycol electrolyte containing 0.05 mol/L ammonium fluoride at 60 V for 1 h, utilizing a platinum coil counter electrode. The as-obtained specimen was sequentially rinsed with deionized water and ethanol, desiccated, and immersed at 60 °C for 24 h to produce TiO_{2-x} exhibiting a bandgap of 2.71 eV. Photoelectrodes fabricated from this reduced material demonstrated photocurrent densities of 91.7

μA/cm², representing nearly fourfold enhancement relative to unmodified TiO_2 anode counterparts. This electrochemical synthesis method can prepare TiO_{2-x} in a short time, and the thickness and morphology can be effectively controlled by precisely adjusting current intensity and deposition time, with good controllability and repeatability.

3.3 Oxidation of Low-Valent Ti Compounds

The oxidation strategy employing low-valent titanium compounds utilizes precursors such as metallic Ti, titanium hydride, and titanium monoxide as starting materials, incorporating Ti^{3+} or H^+ into the crystalline lattice to generate TiO_{2-x} exhibiting a surface-disordered core-shell morphology. Liu et al. [42] combined hydrogen peroxide with titanium hydride to produce a yellow-green gel precursor, which was subsequently desiccated and thermally treated under argon flow (20 mL/min, 5 °C/min heating rate) to yield TiO_{2-x}. Relative to unmodified TiO_2, the reduced material demonstrated pronounced visible-light absorption across the 400–800 nm spectral region, with methylene blue photocatalytic degradation efficiency surpassing commercial TiO_2 by a factor of 68. Reddy et al.[43] placed TiO_2 under a high O_2 flow of 5 L/min and annealed it at 450 °C for 25 min to prepare TiO_{2-x} with good thermal stability. Although the oxidation method of low-valent Ti compounds uses a variety of low-valent Ti compounds as starting materials, providing more options for the preparation process, it may introduce other impurities during preparation, which need to be removed during oxidation, undoubtedly increasing the complexity and cost of preparation.

3.4 Other Emerging Methods

With in-depth research, other novel synthesis methods continue to emerge. Su et al. [44] employed pulsed laser irradiation methodology, processing the TiO_2 surface at a scan velocity of 10 mm/s, resulting in a chromatic transition from white to black. The resultant material exhibited substantially amplified photon harvesting across both visible and near-infrared spectral domains. During pulsed laser irradiation, the high-energy laser beam interacts with the TiO_2 target surface, causing local high temperatures, from which lattice oxygen atoms escape to form oxygen vacancies, improving photocatalytic performance. Jedsukontorn et al.[45] prepared TiO_{2-x} via spark erosion synthesis by reducing metallic titanium under a spark pulse frequency of 20 kHz and a duration of 2 μs. The minimum bandgap was 2.44 eV. Studies show that its light absorption capacity gradually extends to higher absorbance values with prolonged ultrasonic treatment time. During electrical discharge machining, electrode discharge generates high temperature and high pressure, causing the chemical bonds on the TiO_2 surface to break and form oxygen vacancies. Raes et al.[46] used an ultrasonic synthesis method with a power density of 8000 W/L to treat TiO_2 for different durations. The powder color gradually deepened with the increase of ultrasonic treatment time, as shown in Figure 4, mainly because the ultrasonic cavitation effect caused the sample color to deepen with prolonged ultrasonic time, and the wavelength of absorbed light shifted to higher values. After 7 h of treatment, the photocatalytic performance doubled.

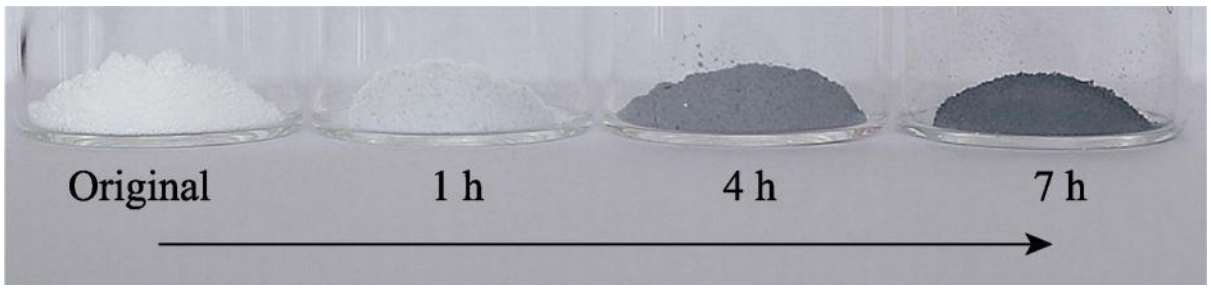

Figure 4 Color variation of TiO_{2-x} prepared by ultrasonic synthesis method with time [46]

In summary, by comparing synthesis principles, advantages, and disadvantages, it is found that high-temperature calcination reduction has high energy consumption and complex operation; electrochemical synthesis cannot prepare powdered TiO_{2-x}; pulsed laser irradiation requires high equipment investment. Table 2 compares the processes of high-temperature calcination reduction, electrochemical synthesis, low-valent Ti compound oxidation, and other emerging synthesis methods, including synthesis principles and advantages/disadvantages. In addition, it is also challenging to determine the appropriate and effective synthesis method of TiO_{2-x} with high defects for different application fields. Therefore, exploring simple, safe, energy-efficient, high-efficiency, and

universal synthesis methods, as well as designing and introducing surface defects for specific application fields to effectively control morphology and particle size, remain the focus of future research.

Table 2 Process comparison of synthesis methods of TiO_{2-x}

Method	Synthesis principle	Advantages and disadvantages	Reference
High-temperature calcination reduction	TiO_2 is reduced under high-temperature conditions. By controlling calcination temperature, time, and atmosphere, Ti^{4+} is reduced to Ti^{3+}, forming defects such as oxygen vacancies.	Advantages: Relatively mature preparation process. Disadvantages: High energy consumption, complex operation, difficult to control product morphology and performance, unsuitable for industrial production.	[8,29-38]
Electrochemical synthesis	An external voltage is applied in the electrolyte to induce anodic oxidation of the Ti sheet to obtain TiO_{2-x}.	Advantages: Mild reaction conditions, easy to control, suitable for preparing high-purity TiO_{2-x}. Disadvantages: High equipment investment and cost, preparation efficiency limited by electrode materials and electrolysis conditions, unable to reduce powdered TiO_2.	[40-41]
Oxidation of low-valent Ti compounds	Oxidizing low-valent Ti compounds to obtain TiO_{2-x} containing Ti^{3+}.	Advantages: Wide sources of raw materials, mild reaction conditions, suitable for preparing powders and films. Disadvantages: Side products may be generated during oxidation, affecting purity and performance.	[42-43]
Other novel synthesis methods	Local high temperature causes oxygen atoms to escape from the lattice, resulting in oxygen vacancies to obtain TiO_{2-x}.	Advantages: Fast reaction speed, high purity. Disadvantages: High equipment requirements and high energy consumption, further exploration needed for film production.	[44-46]

4 Modification Strategies of TiO_{2-x}

Although TiO_{2-x} outperforms traditional TiO_2 in terms of light absorption and photocatalytic performance, its single form still shows limited performance in practical applications. To further improve photocatalytic performance and stability, strategies such as metal loading, non-metal doping, heterojunction construction, and compounding with adsorbent materials have been developed to optimize the performance of TiO_{2-x} for specific reaction systems.

4.1 Metal Loading

Metal nanoparticle decoration can amplify photocatalytic efficiency through exploitation of surface plasmon resonance phenomena and facilitation of photogenerated charge carrier separation. The underlying mechanism is schematically illustrated in Figure 5a [47]: a fraction of the photogenerated electrons migrates to the copper co-catalyst, thereby diminishing the recombination probability of photoexcited charge carriers. Bi et al.[48] prepared TiO_{2-x} via the dual-zone Al reduction method, and then loaded gold nanoparticles (AuNPs) on it via a modified deposition-precipitation method. This process generated a large number of surface oxygen vacancies while significantly promoting the separation and transport of photogenerated electron-hole pairs. As shown in Figure 5b, the benzylacetylene conversion rate of the Au/TiO_2 photocatalyst was only 3.2% under visible light, while that of the Au/TiO_{2-x} catalyst reached up to 43.1%.

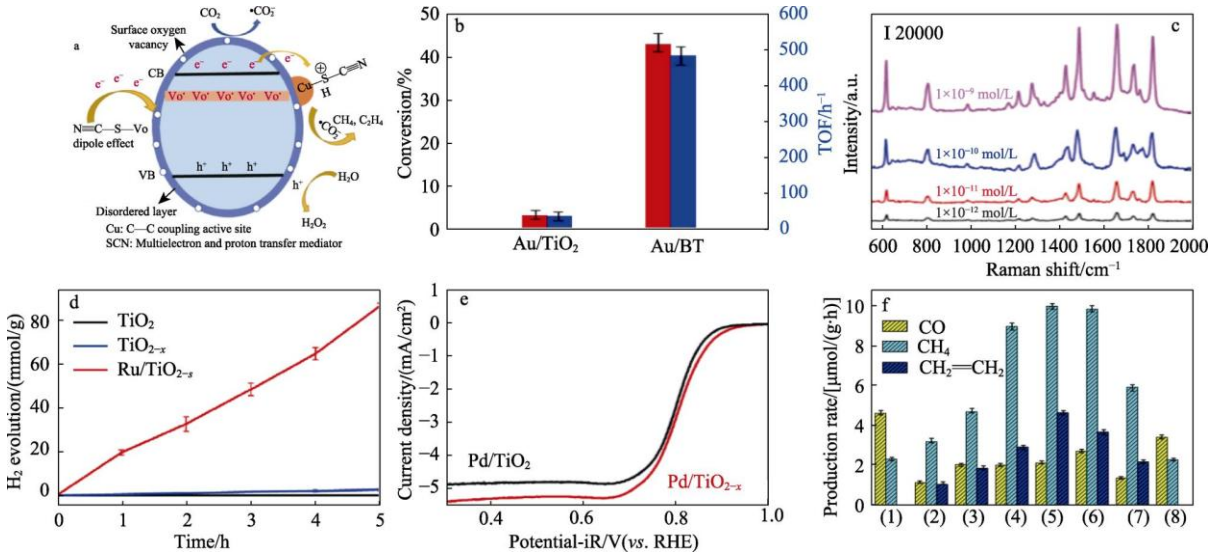

Figure 5 Schematic diagram of mechanism of metal load (a) and performance comparison of Au load (b), Ag load (c), Ru load (d), Pd load (e) and Cu load (f) [47-51]

Cong et al.[49] added TiO_{2-x} to silver nitrate solution under UV/Vis irradiation, stirred and washed it to obtain Ag-loaded TiO_{2-x} substrates (Ag/b-TiO_2). Compared with Ag-loaded TiO_2 (Ag/TiO_2), this material had higher sensitivity: As illustrated in Figure 5c, the detection threshold for rhodamine 6G was as low as 1×10^{-12} mol/L. Yuan et al. [50] immobilized single-atom ruthenium onto hydrogen plasma-reduced TiO_{2-x} through impregnation methodology, yielding Ru/TiO_{2-x}. As depicted in Figure 5d, ruthenium incorporation elevated the hydrogen evolution rate from 0.38 mmol/(g·h) for pristine TiO_{2-x} to 17.81 mmol/(g·h) for the Ru-decorated counterpart (values normalized per catalyst mass). Density functional theory simulations and photoelectrochemical characterization demonstrated that ruthenium introduction generates mid-gap impurity states functioning as electron trapping centers, thereby promoting photogenerated charge separation and transport. Yuan et al. [51] ultrasonically dispersed $PdCl_2$ with TiO_2 in acidic medium, followed by sodium borohydride reduction to obtain Pd/TiO_{2-x}. As shown in Figure 5e, this material exhibited superior catalytic activity, diminished overpotential, and enhanced limiting current density relative to Pd/TiO_2, attributable primarily to palladium surface plasmon resonance and synergistic electronic interactions. Zhang et al. [47] employed copper nitrate as the metal precursor and fabricated a series of high-performance Cu/TiO_{2-x} photocatalysts via photoinduced deposition. Copper functions dually as a co-catalyst suppressing photogenerated carrier recombination and as the active site for photoreduction of CO_2 to hydrocarbon products, thereby enhancing photocatalytic CO_2 conversion efficiency. The maximal production rates for methane and ethylene following copper loading reached 9.9 and 4.8 μmol/(g·h), respectively, as presented in Figure 5f.

Collectively, metal nanoparticle decoration substantially enhances the photocatalytic performance of TiO_{2-x} by markedly promoting photogenerated electron-hole pair separation and migration, thereby elevating overall photocatalytic efficiency. The incorporation of diverse metallic species—including Au, Ag, Ru, Pd, and Cu—not only furnishes additional charge trapping centers but also amplifies the intrinsic catalytic activity of the composite material.

4.2 Non-Metal Doping/Compounding

Non-metal incorporation modifies the electronic configuration of TiO_{2-x}, broadens its spectral absorption window, and compresses the bandgap, thereby enhancing photocatalytic performance. Yang et al. [52] subjected aluminum-reduced TiO_{2-x} to sulfur vapor at elevated temperature for 4 h, introducing sulfur dopants into the oxygen-deficient surface shell to yield R'-TiO_2-S. This material demonstrated substantially amplified photon harvesting across visible and near-infrared regions, with the bandgap narrowed to 0.6 eV. As illustrated in Figure 6a, R'-TiO_2-S achieved near-complete methyl orange degradation within 4 h, whereas pristine TiO_2 (R-TiO_2) exhibited negligible decolorization. The sulfur dopant functions as an electron trap, capturing photogenerated electrons from TiO_{2-x} and thereby promoting charge carrier separation. Rahman et al. [53] initially hydrolyzed

titanium tetrachloride in aqueous glycerol medium to generate titanium hydroxide colloid, subsequently introduced ammonium hydroxide, and calcined the product at 300 °C for 1 h to obtain carbon-doped CB-TiO_2. Adding a certain amount of urea to the colloid yielded C- and N-co-doped CNB-TiO_2. Both showed high photocatalytic performance: as shown in Figure 6b, their bandgaps were reduced to 2.63 and 2.06 eV, respectively. This phenomenon arises because carbon and nitrogen incorporation introduces novel electronic states within the TiO_{2-x} bandgap, compressing its width while functioning as electron donors or acceptors to generate supplementary charge carriers, thereby enhancing photocatalytic efficiency. Furthermore, TiO_{2-x} photocatalytic performance can be augmented through hybridization with graphene quantum dots. Shafiee et al. [54] synthesized TiO_{2-x} via chemical reduction methodology, subsequently ultrasonically dispersing graphene quantum dots with the reduced titania to fabricate GQD-TiO_{2-x} composite photocatalysts. Results show that the bandgap of the composite increased from 2.36 eV to 3.05 eV, as shown in Figure 6c. GQDs act as co-catalysts, transferring light energy to TiO_{2-x} to increase light harvesting efficiency, and GQDs can independently photocatalytically generate reactive species. Concurrently, at the heterojunction interface between graphene quantum dots and the photocatalyst, the GQDs facilitate enhanced separation of photogenerated electron-hole pairs, thereby elevating overall photocatalytic efficiency.

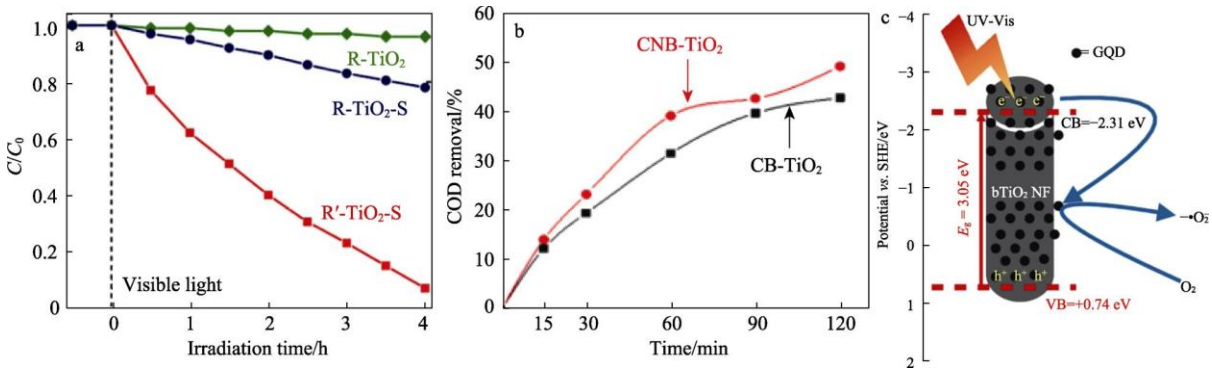

Figure 6 Properties comparison of non-metallic S-doped (a) [52], C and N-doped (b) [53], and schematic diagram of mechanism of black TiO_2 nanofiber ($bTiO_2$ NF)-graphene quantum dot composites (c) [54]

Based on the excellent performance of non-metal-doped TiO_{2-x}, future research should focus on precisely controlling the doping type, concentration, and method to further optimize the performance of TiO_{2-x}, making it applicable to more fields.

4.3 Heterojunction Construction

Rational architectural design of TiO_{2-x} heterojunction configurations can suppress photogenerated electron-hole pair recombination through interfacial charge transfer mechanisms, optimize electron migration pathways, and enhance catalytic activity, thereby preserving material performance under sustained high-efficiency operational conditions. Cui et al. [57] fabricated a TiO_{2-x}/indium oxide S-scheme heterojunction (IO-B-TiO_2/In_2O_3) exhibiting a three-dimensional porous inverse opal architecture. The carbon monoxide evolution rate for this heterojunction photocatalyst reached 162.5 μmol/(g·h), representing a 1.6-fold improvement over the unreduced heterojunction counterpart, as depicted in Figure 7a. Photogenerated electrons migrate from the TiO_{2-x} conduction band to the In_2O_3 valence band across the heterojunction interface, establishing a space charge region that promotes efficient charge carrier separation. This endows the composite material with superior photocatalytic activity, full-spectrum photoresponse, and rapid charge separation and transport kinetics. As a new photocatalyst structure, the S-scheme heterojunction can maximize the redox capacity required for photocatalytic reactions.

DOI:

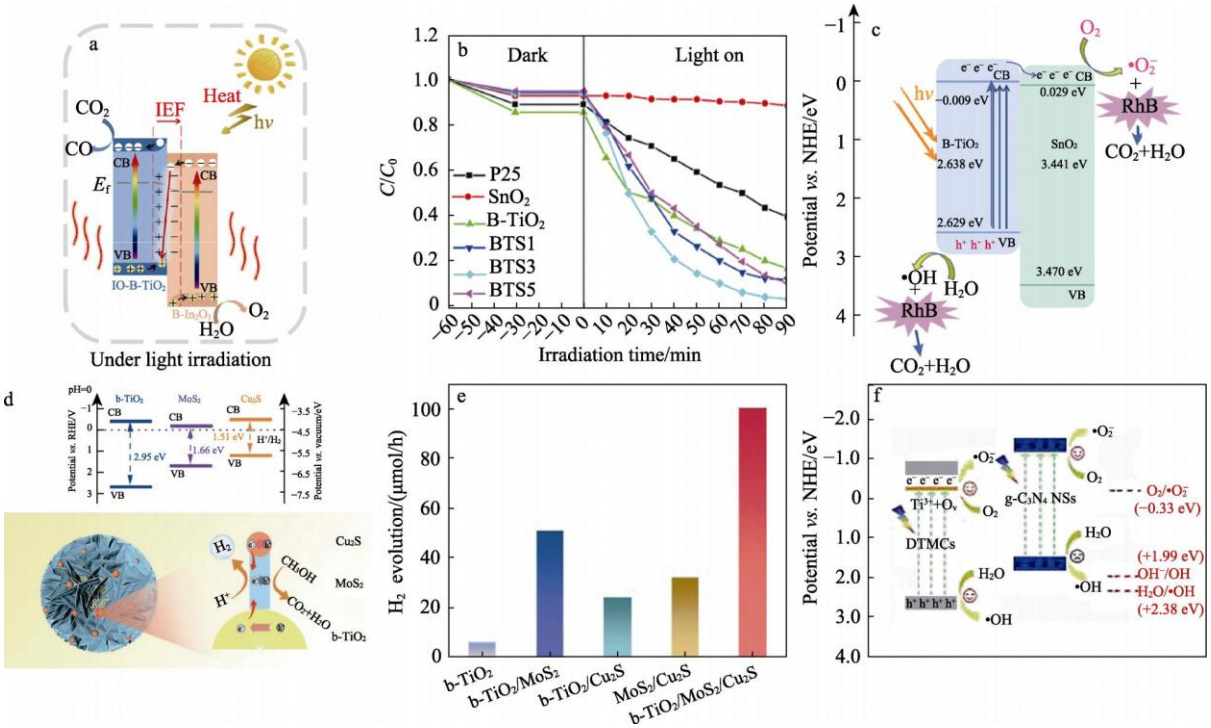

Figure 7 Schematic diagram of S-type heterojunction (a) [57], photocatalytic performance (b) and schematic diagram of type II heterojunction (c) [58], schematic diagram of hierarchical tandem heterojunction (d) and its hydrogen evolution rate (e) [59], and schematic diagram of photocatalytic mechanism Z-type heterojunction (f) [60]

Li et al.[58] prepared a type-II heterojunction (BTS) by chemically combining SnO_2 with TiO_{2-x} prepared via the magnesiothermic reduction method. As illustrated in Figure 7b, the BTS3 composite achieved the highest rhodamine B degradation efficiency at 96.62%, whereas pristine TiO_{2-x} exhibited merely 80% removal. The underlying photocatalytic mechanism is schematically presented in Figure 7c: given that the SnO_2 conduction band edge (0.029 eV) lies below that of TiO_{2-x} (-0.009 eV), photogenerated electrons in the TiO_{2-x} conduction band preferentially migrate to the SnO_2 conduction band. Consequently, the type-II heterojunction synergism effectively enhances photogenerated electron-hole pair separation efficiency and promotes charge carrier transport kinetics.

Li et al.[59] used the solvothermal method to load MoS_2 and Cu_2S nanobelts on the surface of TiO_{2-x} microspheres prepared via high-temperature calcination, obtaining a $TiO_{2-x}/MoS_2/Cu_2S$ hierarchical tandem heterojunction. As depicted in Figure 7d, TiO_{2-x} serves as an effective electron donor material, Cu_2S with its narrow bandgap of 1.51 eV functions as an exceptional light harvester and electron source, while MoS_2 operates as an electron acceptor and transport conduit, collectively extending the photon absorption window of the overall heterojunction architecture. As presented in Figure 7e, the $TiO_{2-x}/MoS_2/Cu_2S$ ternary composite achieved a hydrogen evolution rate of 101.3 μmol/h, substantially surpassing that of single-component TiO_{2-x}. Tan et al.[60] used g-C_3N_4 as the substrate to guide the growth of defective TiO_{2-x} crystalline heterojunctions, successfully preparing a Z-scheme TiO_{2-x}/g-C_3N_4 heterojunction. Results show that the degradation rate of this heterojunction for MO was higher than that of single TiO_{2-x} nanoparticles (DTMCs). As illustrated in Figure 7f, photogenerated electrons residing in the DTMCs conduction band undergo direct recombination with valence band holes in g-C_3N_4 across the heterointerface, markedly enhancing charge carrier separation and thereby amplifying photocatalytic efficiency.

In summary, constructing heterojunctions introduces different lattices and electronic energy levels, which can accelerate electron transport and enhance light absorption capacity, thereby improving photocatalytic performance.

4.4 Compounding with Adsorbent Materials

Adsorbent materials such as activated carbon, coconut shell biomass charcoal, and natural kaolinite have been widely used in environmental pollution control due to their excellent adsorption performance. These materials usually have the characteristics of high conductivity, large specific surface area, and environmental friendliness, providing ideal substrates for constructing high-efficiency photocatalytic composites. However, as a photocatalytic material, TiO_{2-x} has problems such as small particle size, easy agglomeration, low separation efficiency of electron-hole pairs, and poor cycling stability. To overcome these defects, TiO_{2-x} is compounded with adsorbent materials to form new composites with synergistic adsorption and photocatalytic effects. On one hand, the incorporation of adsorbent materials substantially enhances photogenerated electron transport efficiency in TiO_{2-x} while diminishing electron-hole pair recombination probability; on the other hand, the expansive specific surface area of adsorbent substrates furnishes abundant sorption sites, facilitating improved contact probability between target pollutants and the photocatalytic active phase, thereby accelerating the overall photocatalytic reaction kinetics. In addition, as a carrier, adsorbent materials can effectively alleviate the agglomeration problem of TiO_{2-x} particles, thereby improving the dispersion and stability of the material.

Li et al.[61] used the sol-gel method to mix pretreated activated carbon (AC), anhydrous ethanol, tetrabutyl titanate, glacial acetic acid, and acetic acid in proportion, stirred to form a transparent hydrogel, dried and ground into powder, and calcined at 500 °C to prepare TiO_{2-x}/AC composites. The degradation efficiency for RhB was improved by more than 20% (Figure 8a). As shown in Figure 8b, AC provides electron transport channels and reduces the recombination rate, showing far higher photocatalytic degradation capacity than using AC or TiO_{2-x} alone. As shown in Figure 8c, its photocatalytic performance did not decrease significantly after 4 cycles of use, because TiO_{2-x} was loaded on the AC surface, which improved its dispersion and stability. Zakaria et al.[62] dispersed TiO_{2-x}, TiN, and coconut biochar (ACB) in 50 mL ethanol at a mass ratio of 1:1:5, stirred for 2 h, and then calcined to prepare TiO_{2-x}/TiN@ACB composites. ACB, TiN, and TiO_{2-x} formed a synergistic effect, which promoted the separation and transport of photogenerated electrons and holes. As shown in Figure 8d, the catalytic performance of the composite was significantly improved, and it showed excellent stability: as shown in Figure 8e, the performance decreased by ≤3% after 3 cycles of use. Hu et al.[63] used the hydrothermal method to prepare natural kaolinite-modified TiO_{2-x} composites. The modified material achieved a 100% removal rate for MB, far higher than the 32% of single TiO_{2-x}. As shown in Figure 8f, after kaolinite modification, the porous composite formed Al(Si)O-Ti bonds, uniformly fixing TiO_{2-x} on the kaolinite surface, improving its dispersion and increasing the active centers of TiO_{2-x}.

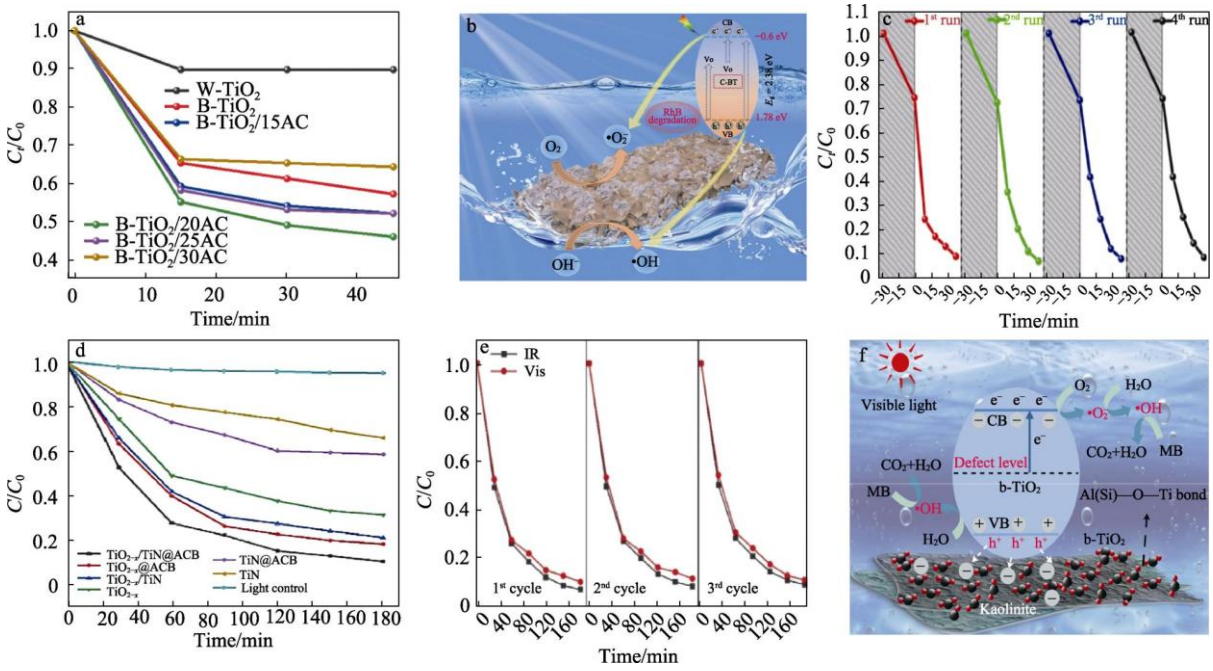

Figure 8 Photocatalytic properties (a), mechanism (b) and number of cycles (c) of TiO_{2-x}/AC composites [61]; Photocatalytic performance (d) and number of cycles (e) of TiO_{2-x}/TiN@ACB [62]; Schematic diagram of mechanism of action of kaolinite-modified TiO_{2-x} (f) [63]

Collectively, hybridizing adsorbent materials with TiO_{2-x} substantially enhances the photocatalytic performance of the reduced titania. The electrical conductivity and expansive specific surface area contributed by the adsorbent phase effectively promote photogenerated electron-hole pair separation efficiency while concurrently mitigating particle aggregation tendencies inherent to TiO_{2-x}. These characteristics make adsorption-photocatalysis synergistic composites show broad application prospects in the removal of aquatic pollutants.

5 Application and Mechanism of TiO_{2-x} and Its Composites in Photocatalytic Degradation of Aquatic Pollutants

Photocatalytic technology for degrading aquatic pollutants is an environmentally friendly treatment technology that does not produce secondary pollutants. Since TiO_{2-x} and its composites break through the limitation that traditional TiO_2 only absorbs ultraviolet light, and have full-spectrum absorption capacity, they have high degradation capacity for a variety of aquatic pollutants, such as dyes, phenolic compounds, pharmaceuticals, and other pollutants.

5.1 Degradation of Dyes

Dyes such as MB, RhB, and MO are widely used in daily life and industrial production. Improper discharge of dye-laden effluent inevitably inflicts severe harm upon both human health and ecological systems. Employing TiO_{2-x} as a photocatalytic agent for dye degradation represents an efficient and environmentally benign approach [64–65]. The underlying mechanism is schematically illustrated in Figure 9. Photocatalytic dye decomposition by pristine TiO_2 encompasses sequential processes including photon absorption, electron-hole pair generation, reactive oxygen species formation, and oxidative cleavage of dye chromophores. Upon illumination by an appropriate light source, TiO_{2-x} harvests photonic energy, promoting valence band electrons (e^-) to the conduction band while generating corresponding holes (h^+) in the valence band region, thereby establishing electron-hole pairs. These charge carriers subsequently engage with surface-adsorbed hydroxyl anions (OH^-) and dissolved molecular oxygen to produce potent oxidizing intermediates including hydroxyl radicals (·OH) and superoxide anion radicals ($\cdot O_2^-$). Finally, the generated multiple radical reactive species undergo addition, substitution, electron transfer, and other reactions with dyes, degrading dyes into small-molecule organics and inorganic substances. Different dyes may form different intermediates, but the overall degradation mechanism still follows redox reactions [66].

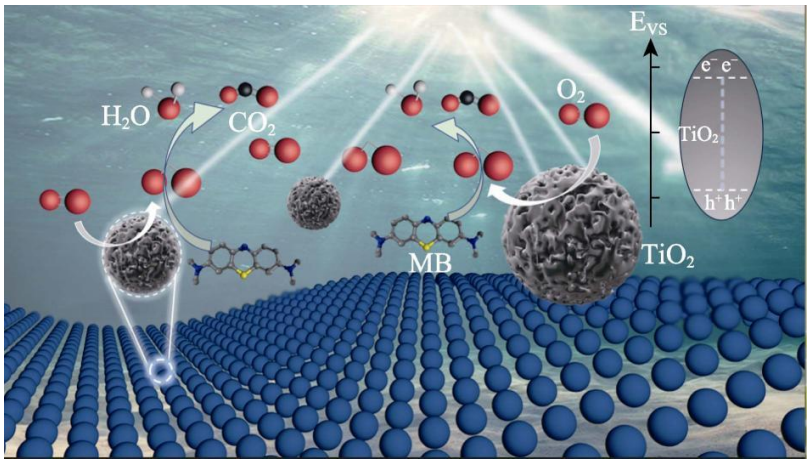

Figure 9 Schematic diagram of TiO_{2-x} photocatalytic degradation of MB

Zhai et al.[67] prepared TiO_{2-x} coatings with pore structures and high photocatalytic activity via suspension plasma spraying technology. Under visible-light illumination, the material achieved 89% degradation efficiency for methylene blue at 5 mg/L mass concentration. Chen et al. [68] synthesized TiO_{2-x} through ethanol-mediated reduction of TiO_2 under ultraviolet lamp exposure, which achieved near-complete rhodamine B degradation (4×10^{-5} mol/L) within 65 min under UV irradiation. Saensook et al. [69] prepared TiO_{2-x} via high-temperature calcination reduction, attaining methyl orange degradation rates of 71.92% under visible light and 82.17% under

ultraviolet light. In addition, composites made from TiO_{2-x} also show excellent performance in dye degradation.

The mechanism of heterojunction photocatalytic degradation of dyes is mainly based on photocatalytic reactions and the performance improvement effect of heterojunctions on photocatalysis. Yuan et al.[70] prepared a N-doped TiO_{2-x} and g-C_3N_4 three-phase heterojunction (N-Ti^{3+}-TiO_2/g-C_3N_4) via solvothermal synthesis. Under visible light, its degradation rate for MB with a mass concentration of 5 mg/L reached 81% within 100 min. Among these, Ti^{3+} generates an intermediate electronic state near the conduction band minimum of TiO_2, whereas nitrogen incorporation establishes impurity levels proximal to the valence band maximum. Photoexcited electrons can thus be promoted from either the TiO_2 valence band or the nitrogen 2p orbitals to the Ti^{3+} mid-gap states. Consequently, photogenerated electrons originating from g-C_3N_4 are more readily transferred to the conduction band of the N/Ti^{3+} co-doped ternary architecture. The resultant hydroxyl and superoxide radicals constitute the primary oxidative species responsible for methylene blue degradation. Chen et al. [71] synthesized a Ti^{3+} self-doped Ag_2O/TiO_2 p-n nanoheterojunction through photochemical reaction of silver nitrate with TiO_2 under 500 W xenon lamp irradiation. Under visible-light conditions, rhodamine B degradation efficiency exceeded 90% within 150 min for an initial concentration of 10 mg/L. Within this system, Ag_2O functions as the p-type semiconductor and TiO_{2-x} as the n-type counterpart. Electron migration from n-type TiO_{2-x} to p-type Ag_2O proceeds until Fermi level equilibration is achieved, establishing a built-in electric field that accelerates photogenerated charge carrier separation and thereby enhances rhodamine B photocatalytic degradation.

The photocatalytic mechanism of TiO_{2-x} composites with adsorbent materials is based on the fact that adsorbent materials provide additional electron transport channels or reaction active sites, promote the separation of photogenerated electrons and holes, and inhibit their recombination, thereby enhancing the degradation performance for dye molecules. Wang et al.[72] prepared TiO_{2-x} compounded with reduced graphene oxide (RGO) via the solvothermal method. Under visible light, it completely degraded MB with a mass concentration of 40 mg/L within 120 min. After compounding TiO_{2-x} with RGO, photogenerated electrons on the conduction band of TiO_{2-x} transfer to the RGO surface, promoting the separation of electron-hole pairs. The generated ·OH and h^+ are the main reactive species for MB degradation. Li et al.[73] prepared TiO_{2-x}/AC via the sol-gel method, which degraded RhB with a mass concentration of 2 mg/L by 92% within 60 min under visible light. AC acts as a good electron transfer channel, rapidly transferring electrons and effectively enhancing photocatalytic performance. ·OH and $\cdot O_2^-$ are the main reactive species for RhB degradation. Table 3 summarizes the performance of TiO_{2-x} and different composites in dye degradation in recent years.

5.2 Degradation of Phenolic Compounds

Phenolic compounds are widely present in wastewater from petrochemical, printing and dyeing, pesticide, and other industries. They have high solubility and easy migration, and will cause serious toxic effects on organisms when their concentration reaches a certain threshold. The utilization of TiO_{2-x} and its composite derivatives for phenolic compound degradation offers substantial merits including elevated removal efficiency, absence of secondary contamination, and diminished energy requirements [82].

Nawaz et al.[83] prepared colored TiO_2 via a glycerol-mediated solvothermal method, and used it to photocatalytically degrade total phenolic compounds extracted from palm oil mill effluent (POME). Under visible light, the generated reactive species could open the ring of total phenolic compounds and degrade them into harmless small molecules. The degradation efficiency for simulated wastewater at an initial concentration of 800 mg/L reached 48.17% within 180 min. Han et al. [84] synthesized TiO_{2-x} through solvothermal methodology, achieving phenol degradation rates under visible light that were 5.2-fold higher than pristine TiO_2 for an initial concentration of 200 mg/L. Zhou et al. [85] fabricated Ag/TiO_{2-x} composites, which eliminated over 99% of 2,4-dichlorophenol at 5 mg/L initial concentration within 2 h under visible-light irradiation. Within this system, silver nanoparticles facilitated photogenerated electron transfer to the TiO_{2-x} conduction band through surface plasmon resonance, thereby enhancing photocatalytic efficiency. The principal reactive species responsible for 2,4-dichlorophenol mineralization were hydroxyl and superoxide radicals. Qiao et al. [86] prepared Ag/TiO_{2-x} nanotube heterojunctions via wet impregnation combined with photoreduction methodology. Under visible-near-infrared light, it completely mineralized 4-nitrophenol within 70 s. The photocatalytic mechanism schematic is shown in Figure 10: ·OH generated by TiO_{2-x} oxidizes phenolic compounds to form simpler intermediates (such as hydroxyphenol generated during phenol degradation), and Ag accelerates charge separation via the SPR effect

to enhance this process. Then, after multi-step oxidation and ring-opening reactions, it is finally converted into small-molecule organics and inorganic substances such as CO_2 and H_2O. Results show that different modification strategies, such as doping and compounding, can significantly improve the photocatalytic degradation performance of TiO_{2-x} for phenolic compounds. Future research should further optimize the material structure and stability to improve degradation efficiency.

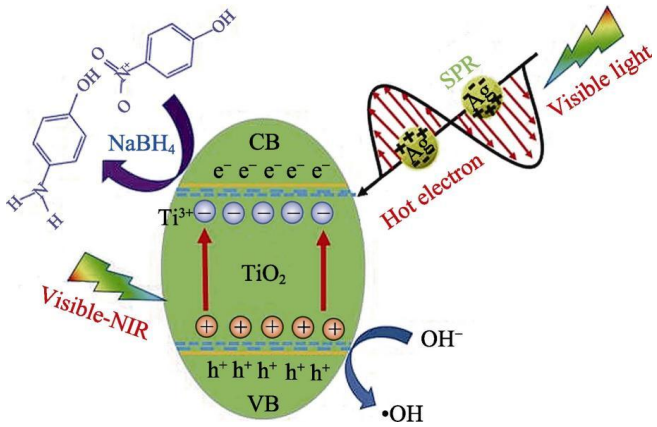

Figure 10 Schematic diagram of photocatalytic mechanism of Ag/TiO_{2-x} nanotube heterojunction [86]

5.3 Degradation of Pharmaceuticals

Pharmaceuticals such as antibiotic residues in water bodies will inhibit or kill microorganisms in water and destroy the ecological balance. TiO_{2-x} and its composites provide an efficient and environmentally friendly solution for pharmaceutical degradation [87]. Bazzanella et al.[88] prepared TiO_{2-x} via ethanol reduction of TiO_2, and used it to degrade ciprofloxacin with an initial mass concentration of 10 mg/L. The degradation rate reached 95% within 60 min. The degradation mainly involved decarboxylation and deacetylation of ciprofloxacin by h^+ and ·OH generated during the TiO_{2-x} photocatalytic process, reducing the relative molecular mass. Feng et al. [89] fabricated an oxygen-vacancy and phosphorus co-doped TiO_2-coated carbon nanotube composite (OVPTCN) through a sequential solvothermal-phosphorization approach. This material achieved 87% degradation efficiency for acetaminophen solution at an initial concentration of 5 mg/L within 40 min. Phosphorus incorporation compressed the bandgap and amplified photon harvesting capability. The dominant reactive species were photogenerated holes and hydroxyl radicals produced during composite photocatalysis, which initiated hydroxylation of acetaminophen molecules. Wu et al.[90] prepared TiO_{2-x} via high-temperature hydrogenation reduction, and its degradation rate for tetracycline with an initial mass concentration of 10 mg/L reached 66.2% within 240 min. The degradation mechanism was the redox reaction of tetracycline by $\cdot O_2^-$ and h^+ generated by photocatalysis. Ren et al.[91] prepared a heterojunction of TiO_{2-x} and γ-Fe_2O_3 ultrathin nanosheets via hydrogenation reduction. Its degradation rate for tetracycline with an initial mass concentration of 10 mg/L reached 99.3% within 50 min. Photogenerated electrons on the conduction band of TiO_{2-x} easily transferred to Fe_2O_3, leading to the formation of more $\cdot O_2^-$ on the surface, accelerating the separation of electron-hole pairs, thereby enhancing photocatalytic performance. Masking experiments and characterizations show that ·OH, $\cdot O_2^-$, and H_2O_2 generated by this heterojunction attack the phenolic and amino groups in tetracycline molecules with high electron cloud density, obtaining a series of small-molecule intermediates, and finally being oxidized to carboxylic acids to achieve degradation. He et al. [92] fabricated a ternary heterocomposite (RGO/B-TiO_2/2D-ZIF-8) through polyvinylpyrrolidone-mediated integration of reduced graphene oxide, black TiO_2 nanosheets, and two-dimensional ZIF-8 sheets. Under xenon lamp irradiation, this material achieved 76% degradation efficiency for doxycycline hydrochloride at an initial concentration of 25 mg/L within 120 min. Under visible-light conditions, photogenerated electrons in the 2D-ZIF-8 conduction band migrate to the TiO_{2-x} conduction band, while holes in the TiO_{2-x} valence band transfer to 2D-ZIF-8. Given that the $O_2/\cdot O_2^-$ redox potential (±0.33 eV vs. NHE) is more negative than the TiO_{2-x} conduction band edge, surface electrons cannot reduce molecular oxygen to superoxide radicals. Simultaneously, the 2D-ZIF-8 valence band position (0.34 eV) is insufficiently positive relative to the H_2O/OH^- potential (2.53 eV vs. NHE), precluding hole-mediated hydroxyl radical generation from water. Consequently, direct hole oxidation of doxycycline hydrochloride constitutes the sole degradation pathway.

Overall, the photocatalytic degradation of pharmaceutical molecules by TiO_{2-x} and its composites involves the oxidative degradation of pharmaceutical pollutants by different reactive species, and achieves pharmaceutical degradation and mineralization through pathways such as hydroxylation and ring opening of molecular structures.

5.4 Degradation of Other Pollutants

TiO_{2-x} and its composites also have high degradation rates for removing heavy metals [such as Cr(VI)] and organic pollutants (such as aniline). Cao et al.[93] prepared black mesoporous TiO_{2-x} via sodium borohydride reduction, and its removal rate for Cr(VI) with an initial mass concentration of 5 mg/L reached 95% within 210 min under visible light. Yan et al. [94] synthesized TiO_{2-x} featuring a microporous shell architecture through sodium borohydride reduction, achieving 92.3% removal efficiency for hexavalent chromium at an initial concentration of 20 mg/L within 60 min under visible-light irradiation. The underlying mechanism likely involves photogenerated electrons produced by TiO_{2-x} under visible-light exposure reducing dissolved Cr(VI) to Cr(III), which subsequently precipitates as chromium hydroxide [$Cr(OH)_3$], thereby accomplishing Cr(VI) sequestration from the aqueous phase. The removal mechanisms are shown in Equations (1) and (2):

$$Cr2O72-+14H++6(e- CB)\rightarrow 2Cr3++7H2O \quad (1)$$

$$Cr2O72-+7H2O+6(e- CB)\rightarrow 2Cr(OH)3\downarrow+8OH- \quad (2)$$

Li et al. [95] synthesized TiO_{2-x} through mild ion exchange treatment of titanium in an ionic liquid medium containing lithium acetate and acetic acid. Under visible-light irradiation, this material achieved 60% degradation efficiency for aniline at an initial concentration of 10 mg/L within 4 h. The mechanism involves the reaction of C_6H_7N with reactive radicals to generate intermediates such as nitrobenzene and azobenzene, which are gradually converted into small-molecule substances under photocatalysis, and finally mineralized into harmless compounds such as NH_4^+, NO_3^-, and CO_2. The degradation mechanism is shown in Equations (3) and (4):

$$TiO2-x+hv\rightarrow TiO2(h+ VB+e- CB) \quad (3)$$

$$TiO2(h+ VB)/\cdot OH+C6H7N\rightarrow C6H5NO2/C12H10N2\rightarrow NH4++NO3-+CO2\uparrow \quad (4)$$

In summary, when TiO_{2-x} and its composites are used for photocatalytic degradation of aquatic pollutants, the active groups involved change accordingly due to the change of electron transport paths. Therefore, the study of photocatalytic mechanisms is of great significance for controlling the degradation of aquatic pollutants, and also provides a theoretical basis for efficiently removing different pollutants.

6 Conclusions and Prospects

The selection of synthesis conditions for TiO_2 directly determines the color, structure, and performance of the prepared TiO_{2-x}. Its excellent optical, chemical, and electronic properties are attributed to various defects in its structure, such as surface disorder, oxygen vacancies, and Ti^{3+}. Related studies show that TiO_{2-x} has demonstrated good application potential, promoting the continuous optimization and upgrading of its synthesis methods, from dangerous high-temperature H_2 reduction to mild methods using other reducing agents, electrochemical reduction, low-valent Ti compound oxidation, ultrasonic treatment, and laser modification. Despite the enhanced performance characteristics of TiO_{2-x}, its single-component configuration still exhibits limitations in electron transport pathways and visible-light photoresponse that warrant further optimization for practical deployment. Strategic modifications including metal nanoparticle decoration, non-metal incorporation, heterojunction engineering, and adsorbent material hybridization are employed to suppress electron-hole pair recombination and amplify photon harvesting efficiency, thereby expanding its applicability in aqueous pollutant remediation.

Although TiO_{2-x} and its composites have achieved good results in the field of water pollution treatment, their future development still faces many challenges: (1) The preparation of TiO_{2-x} and its composites usually involves multiple steps, including material selection, pretreatment, optimization, and separation, which increases the

complexity and technical requirements of preparation. Therefore, it is urgent to develop TiO_{2-x} composites with more stable structures and simpler processes, and clarify the synergistic mechanism of their photocatalytic active centers. (2) Surface oxygen vacancy generation compresses the bandgap and enhances photocatalytic efficiency; however, the precise control of oxygen vacancy concentration during synthesis remains challenging. Current research indicates that superfluous oxygen vacancies can facilitate photogenerated carrier recombination, consequently diminishing photocatalytic performance. Therefore, it is necessary to explore and develop preparation methods that can precisely control the content of oxygen vacancies, which are environmentally friendly, low-cost, low-energy-consumption, and simple in process flow, such as novel surface modification methods, and combining machine learning to optimize the contents of oxygen vacancies and Ti^{3+}. (3) Based on the excellent performance of TiO_{2-x} and its composites, future research should expand the application in micro-pollutants and emerging pollutants, such as microplastics and endocrine disruptors, which have strong mobility and high toxicity. (4) TiO_{2-x} and its composites are difficult to completely recover from the reaction system in the field of water purification, which limits their application. The development of magnetically recoverable or non-particulate TiO_{2-x} configurations is anticipated to facilitate broader practical implementation and commercial adoption.

Collectively, TiO_{2-x} and its composite derivatives demonstrate promising photocatalytic degradation efficacy, particularly in the remediation of aqueous contaminants. Moving forward, the development of robust yet facile synthesis and optimization protocols remains imperative to enhance material regenerability and industrial scalability, thereby enabling more extensive environmental protection applications.

References

[1] Chen X B, Lu L, Yu P Y, et al. Increasing solar absorption for photocatalysis with black hydrogenated titanium dioxide nanocrystals. Science, 2011, 331(6018): 746-750.

[2] Li N, Zhang W, Li G X, et al. Research progress on TiO_2 photocatalysts. Fine Chemicals, 2021, 38(11): 2181-2188, 2258.

[3] Fuentes K M, Venuti D, Betancourt P. Black titania with increased defective sites for phenol photodegradation under visible light. Reaction Kinetics, Mechanisms and Catalysis, 2020, 131(1): 423-435.

[4] Andronic L, Lelis M, Enesca A, et al. Photocatalytic activity of defective black-titanium oxide photocatalysts towards pesticide degradation under UV/Vis irradiation. Surfaces and Interfaces, 2022, 32: 102123.

[5] Khanam R, Taparia D, Momdal B, et al. Black titania: Effect of hydrogenation on structural and thermal stability of nanotitania. Applied Physics A, 2016, 122(2): 92.

[6] Thakur N, Thakur N, Kumar A, et al. A critical review on the recent trends of photocatalytic, antibacterial, antioxidant and nanohybrid applications of anatase and rutile TiO_2 nanoparticles. Science of the Total Environment, 2021, 914: 169815.

[7] Haidner S, Nawaz R, Anjum M, et al. Property-performance relationship of core-shell structured black TiO_2 photocatalyst for environmental remediation. Frontiers of Environmental Science & Engineering, 2022, 17(9): 111.

[8] Soria J, Sanz J, Torralvo M J, et al. The effect of the surface disordered layer on the photoreactivity of titania nanoparticles. Applied Catalysis B: Environmental, 2017, 210: 306-319.

[9] Li Z, Wang E G, Zhang Y Z, et al. Antibacterial ability of black titania in dark: Via oxygen vacancies mediated electron transfer. Nano Today, 2022, 50: 101826.

[10] Jiang W B, Loh H Y, Low B Q L, et al. Role of oxygen vacancy in metal oxides for photocatalytic CO_2 reduction. Applied Catalysis B: Environmental, 2022, 321: 122079.

[11] Deskins N A, Du J, Rao P. The structural and electronic properties of reduced amorphous titania. Physical Chemistry Chemical Physics, 2017, 19(28): 18671-18684.

[12] Liu X G, Bi Y P. Synergistic effect of Ti^{3+} doping and facet regulation over Ti^{3+}-doped TiO_2 nanosheets with enhanced photoreactivity. Catalysis Science & Technology, 2018, 8(15): 3876-3882.

[13] Abdullah S A, Sahdan M Z, Nafarizal N, et al. Influence of substrate annealing on inducing Ti^{3+} and oxygen vacancy in TiO_2 thin films deposited via RF magnetron sputtering. Applied Surface Science, 2018, 462: 575-582.

[14] Gao X T. Study on photocatalytic properties based on TiO_{2-x} and its composites [D]. Harbin: Harbin Normal University, 2022.

[15] He M, Ji J, Liu B Y, et al. Reduced TiO_2 with tunable oxygen vacancies for catalytic oxidation of formaldehyde at room temperature. Applied Surface Science, 2019, 473: 934-942.
[16] Chen J, Ding Z Y, Wang C, et al. Black anatase titania with ultrafast sodium-storage performances stimulated by oxygen vacancies. ACS Applied Materials & Interfaces, 2016, 8(14): 9142-9151.
[17] Shi D X, Zhang H H, Gao X, et al. Research progress on the preparation and catalytic application of core-shell nanocomposites. Fine Chemicals, 2021, 40(1): 33-43.
[18] Hu W Y, Zhou W, Zhang K F, et al. Facile strategy for controllable synthesis of stable mesoporous black TiO_2 hollow spheres with efficient solar-driven photocatalytic hydrogen evolution. Journal of Materials Chemistry A, 2016, 4(19): 7495-7502.
[19] Zhang K, Park J H. Surface localization of defects in black TiO_2: Enhancing photoactivity or reactivity. The Journal of Physical Chemistry Letters, 2017, 8(1): 199-207.
[20] Zhang S S, Zhang S Q, Peng B Y, et al. High performance hydrogenated TiO_2 nanorod arrays as a photoelectrochemical sensor for organic compounds under visible light. Electrochemistry Communications, 2014, 40: 24-27.
[21] Wang Z, Yang C Y, Lin T, et al. H-doped black titania with very high solar absorption and excellent photocatalysis enhanced by localized surface plasmon resonance. Advanced Functional Materials, 2013, 23(43): 5444-5450.
[22] Pylnev M, Chang W H, Wong M S. Shell of black titania prepared by sputtering TiO_2 target in H_2+Ar plasma. Applied Surface Science, 2018, 462: 285-290.
[23] Ariyanti D, Mills L, Dong J, et al. $NaBH_4$ modified TiO_2: Defect site enhancement related to its photocatalytic activity. Materials Chemistry and Physics, 2017, 199: 571-576.
[24] Chen S H, Xiao Y, Wang Y H, et al. A facile approach to prepare black TiO_2 with oxygen vacancy for enhancing photocatalytic activity. Nanomaterials, 2018, 8(4): 245.
[25] Zheng P, Tang J L, Zhou Z P, et al. Ultrafast synthesis of defective black TiO_2 via one-step NaN_3 deflagration for high-efficiency solar water evaporation. Surfaces and Interfaces, 2020, 22: 100901.
[26] Wang Z, Yang C Y, Lin T Q, et al. Visible-light photocatalytic, solar thermal and photoelectrochemical properties of aluminium-reduced black titania. Energy & Environmental Science, 2013, 6(10): 3007-3014.
[27] Lin L X, Huang J T, Li X F, et al. Effective surface disorder engineering of metal oxide nanocrystals for improved photocatalysis. Applied Catalysis B: Environmental, 2017, 203: 615-624.
[28] Azab N A, El-Sharkawy A A M, Omran Z A, et al. C_3N_4 interlayer formation while synthesizing black titania and their dye sensitized solar cell and conductivity performances. Solar Energy Materials and Solar Cells, 2021, 232: 111347.
[29] Qi W T, Wang N, Chen X Y, et al. Plasmon-assisted partially reduced TiO_2 nanotube arrays for photoelectrochemical water splitting. Materials Research Express, 2020, 6(12): 1250h9.
[30] Li Z B, Bian H D, Xiao X F, et al. Defective black TiO_2 nanotube arrays for enhanced photocatalytic and photoelectrochemical applications. ACS Applied Nano Materials, 2019, 2(11): 7372-7378.
[31] Liu X, Xu H, Grabstanowicz L R, et al. Ti^{3+} self-doped TiO_{2-x} anatase nanoparticles via oxidation of TiH_2 in H_2O_2. Catalysis Today, 2014, 225: 80-89.
[32] Reddy Y A K, Kang I K, Shin Y B, et al. Oxygen atmosphere annealing effect on the thermal stability of TiO_{2-x} based films for shutter-less infrared image sensors. Key Engineering Materials, 2018, 775: 272-277.
[33] Su Y, Zhang W, Chen S M, et al. Engineering black titanium dioxide by femtosecond laser filament. Applied Surface Science, 2020, 520: 146298.
[34] Jedsukontorn T, Ueno T, Saito N, et al. Facile preparation of defective black TiO_2 through the solution plasma process: Effect of parametric changes for plasma discharge on its structural and optical properties. Journal of Alloys and Compounds, 2017, 726: 567-577.
[35] Raes A, Ninakanti R, Van den B L, et al. Black titania by sonochemistry: A critical evaluation of existing methods. Ultrasonics Sonochemistry, 2021, 100: 106601.
[36] Zhang L N, Liu T L, Liu T F, et al. Improving photocatalytic performance of defective titania for carbon dioxide photoreduction by Cu cocatalyst with SCN^- ion modification. Chemical Engineering Journal, 2021, 463: 142358.
[37] Bi Q Y, Song E, Chen J C, et al. Nano gold coupled black titania composites with enhanced surface plasma properties for efficient photocatalytic alkyne reduction. Applied Catalysis B: Environmental, 2022, 309: 121222.
[38] Cong T Z, Zhang Y F, Huang H, et al. Ag nanoparticles synthesized on black-titanium dioxide by photocatalytic method as reusable substrates of surface-enhanced Raman spectroscopy. Chemosensors, 2022, 10(11): 441.

[39] Yuan C F, Shen Y L, Zhu C Y, et al. Ru single-atom decorated black TiO_2 nanosheets for efficient solar-driven hydrogen production. ACS Sustainable Chemistry & Engineering, 2022, 10(31): 10311-10317.
[40] Yuan X T, Wang X, Liu X Y, et al. Ti^{3+}-promoted high oxygen-reduction activity of Pd nanodots supported by black titania nanobelts. ACS Applied Materials & Interfaces, 2016, 8(41): 27654-27660.
[41] Yang C Y, Wang Z, Lin T Q, et al. Core-shell nanostructured "black" rutile titania as excellent catalyst for hydrogen production enhanced by sulfur doping. Journal of the American Chemical Society, 2013, 135(47): 17831-17838.
[42] Rahman S, Nawaz R, Khan J, et al. Synthesis and characterization of carbon and carbon-nitrogen doped black TiO_2 nanomaterials and their application in sonophotocatalytic remediation of treated agro-industrial wastewater. Materials, 2021, 14(20): 6175.
[43] Shafiee A, Carrier A J, Nganou C, et al. Mechanistic insight into the enhanced photodegradation by black titanium dioxide nanofiber-graphene quantum dot composites. Applied Surface Science, 2020, 636: 157836.
[44] Cui H, Cao J Y, Zhao Y, et al. Construction of IO-B-TiO_2/In_2O_3 S-scheme heterojunction with photothermal effects and its highly efficient photocatalytic reduction of CO_2 under full-spectrum light. Chemical Engineering Journal, 2022, 479: 147618.
[45] Li Y F, Feng Y C, Bai H, et al. Enhanced visible-light photocatalytic performance of black TiO_2/SnO_2 nanoparticles. Journal of Alloys and Compounds, 2021, 960: 170672.
[46] Li Z Z, Li H Z, Wang S J, et al. Mesoporous black TiO_2/MoS_2/Cu_2S hierarchical tandem heterojunctions toward optimized photothermal-photocatalytic fuel production. Chemical Engineering Journal, 2022, 427: 131830.
[47] Tan B Y, Ye X Z, Li Y J, et al. Defective anatase TiO_{2-x} mesocrystal growth in situ on g-C_3N_4 nanosheets: Construction of 3D/2D Z-scheme heterostructures for highly efficient visible-light photocatalysis. Chemistry—A European Journal, 2018, 24(50): 13311-13321.
[48] Li J, Jiang Z X, Li J F, et al. Synthesis of black titanium dioxide/activated carbon composites for enhanced visible-light photocatalytic properties. Journal of Materials Science: Materials in Electronics, 2022, 35(16): 1050.
[49] Zakaria H, Li Y, Fathy M M, et al. A novel TiO_{2-x}/TiN@ACB composite for synchronous photocatalytic Cr(VI) reduction and water photothermal evaporation under visible/infrared light illumination. Chemosphere, 2021, 311: 137137.
[50] Hu P W, Zhang Y, Cheng G L. Natural kaolinite modified black titanium dioxide for efficient visible light assisted photocatalysis. Molecular Catalysis, 2021, 547: 113312.
[51] Zhai M J, Liu Y, Huang J, et al. Efficient suspension plasma spray fabrication of black titanium dioxide coatings with visible light absorption performances. Ceramics International, 2019, 45(1): 930-935.
[52] Chen S H, Wang Y H, Li J, et al. Synthesis of black TiO_2 with efficient visible-light photocatalytic activity by ultraviolet light irradiation and low temperature annealing. Materials Research Bulletin, 2018, 98: 280-287.
[53] Saensook S, Sirisuk A. A factorial experimental design approach to obtain defect-rich black TiO_2 for photocatalytic dye degradation. Journal of Water Process Engineering, 2022, 45: 102495.
[54] Yuan X J, Sun M X, Yao Y, et al. N/Ti^{3+}-codoped triphasic TiO_2/g-C_3N_4 heterojunctions as visible-light photocatalysts for the degradation of organic contaminants. New Journal of Chemistry, 2019, 43(6): 2665-2675.
[55] Chen P. A novel synthesis of Ti^{3+} self-doped Ag_2O/TiO_2 (p-n) nanoheterojunctions for enhanced visible photocatalytic activity. Materials Letters, 2016, 163: 130-133.
[56] Wang S C, Cai J S, Mao J J, et al. Defective black Ti^{3+} self-doped TiO_2 and reduced graphene oxide composite nanoparticles for boosting visible-light driven photocatalytic and photoelectrochemical activity. Applied Surface Science, 2019, 467: 45-55.
[57] Jiang X D, Zhang Y P, Jiang J, et al. Characterization of oxygen vacancy associates within hydrogenated TiO_2: A positron annihilation study. The Journal of Physical Chemistry C, 2012, 116(42): 22619-22624.
[58] Pradenas M, Yanez J, Ranganathan S, et al. Multivariate approach to hydrogenated TiO_2 photocatalytic activity under visible light. Water Environment Research, 2019, 91(2): 157-164.
[59] An H R, Park S Y, Kim H, et al. Advanced nanoporous TiO_2 photocatalysts by hydrogen plasma for efficient solar-light photocatalytic application. Scientific Reports, 2016, 6(1): 29683.
[60] Wang X T, Li Y M, Liu X, et al. Preparation of Ti^{3+} self-doped TiO_2 nanoparticles and their visible light photocatalytic activity. Chinese Journal of Catalysis, 2015, 36(3): 389-399.
[61] Han K, Zhang X, Wang H F, et al. A facile microwaving method to turn titanium oxide into highly active Ti^{3+} self-doped structure. Journal of Nanoscience and Nanotechnology, 2016, 16(9): 9826-9831.
[62] Li G L, Li J, Li G, et al. N and Ti^{3+} co-doped 3D anatase TiO_2 superstructures composed of ultrathin nanosheets

with enhanced visible light photocatalytic activity. Journal of Materials Chemistry A, 2015, 3(44): 22073-22080.

[63] Zhang H, Xing Z P, Zhang Y, et al. Ni^{2+} and Ti^{3+} co-doped porous black anatase TiO_2 with unprecedented-high visible-light-driven photocatalytic degradation performance. RSC Advances, 2015, 5(129): 107150-107157.

[64] Du J M, Wang H M, Chen H J, et al. Synthesis and enhanced photocatalytic activity of black porous Zr-doped TiO_2 monoliths. Nano, 2016, 11(6): 1650068.

[65] Nawaz R, Kait C F, Chia H Y, et al. Glycerol-mediated facile synthesis of colored titania nanoparticles for visible light photodegradation of phenolic compounds. Nanomaterials, 2019, 9(11): 1586.

[66] Han L J, Su B T, Liu G, et al. Synthesis of oxygen vacancy-rich black TiO_2 nanoparticles and the visible light photocatalytic performance. Molecular Catalysis, 2018, 456: 96-101.

[67] Zhou G, Meng H Y, Cao Y, et al. Surface plasmon resonance-enhanced solar-driven photocatalytic performance from Ag nanoparticles-decorated Ti^{3+} self-doped porous black TiO_2 pillars. Journal of Industrial and Engineering Chemistry, 2018, 64: 188-193.

[68] Qiao P Z, Sun B J, Li H Z, et al. Surface plasmon resonance-enhanced visible-NIR-driven photocatalytic and photothermal catalytic performance by Ag/mesoporous black TiO_2 nanotube heterojunctions. Chemistry—An Asian Journal, 2019, 14(1): 177-186.

[69] Bazzanella N, Bajpai O P, Fendrich M, et al. Ciprofloxacin degradation with a defective TiO_{2-x} nanomaterial under sunlight. MRS Communications, 2022, 13(6): 1252-1259.

[70] Feng X Y, Wang P F, Hou J, et al. Oxygen vacancies and phosphorus codoped black titania coated carbon nanotube composite photocatalyst with efficient photocatalytic performance for the degradation of acetaminophen under visible light irradiation. Chemical Engineering Journal, 2018, 352: 947-956.

[71] Wu S Q, Li X Y, Tian Y Q, et al. Excellent photocatalytic degradation of tetracycline over black anatase-TiO_2 under visible light. Chemical Engineering Journal, 2021, 406: 126747.

[72] Ren L P, Zhou W, Sun B J, et al. Defects-engineering of magnetic γ-Fe_2O_3 ultrathin nanosheets/mesoporous black TiO_2 hollow sphere heterojunctions for efficient charge separation and the solar-driven photocatalytic mechanism of tetracycline degradation. Applied Catalysis B: Environmental, 2019, 240: 319-328.

[73] He J H, Ye J, Zhang Y, et al. Synergistic RGO/black TiO_2/2D-ZIF-8 ternary heterogeneous composite with highly efficient photocatalytic activity. ChemistrySelect, 2020, 5(12): 3746-3755.

[74] Cao Y, Xing Z P, Hu M Q, et al. Mesoporous black N-TiO_2-hollow spheres as efficient visible-light-driven photocatalysts. Journal of Catalysis, 2017, 356: 246-254.

[75] Yan Z Y, Huang W X, Jiang X R, et al. Hollow structured black TiO_2 with thickness-controllable microporous shells for enhanced visible-light-driven photocatalysis. Microporous and Mesoporous Materials, 2021, 323: 111228.

[76] Li G S, Lian Z C, Li X, et al. Ionothermal synthesis of black Ti^{3+}-doped single-crystal TiO_2 as an active photocatalyst for pollutant degradation and H_2 generation. Journal of Materials Chemistry A, 2015, 3(7): 3748-3756.